RESEARCH ARTICLE

Effect of Mn Substitution on the Electrochemical Properties of LiTi$_2$(PO$_4$)$_3$

A.VENKATESWARA RAO[a*], V.VEERAIAH[a],
A.V.PRASADA RAO[b] and B.KISHORE BABU[c]

[a]Department of Physics, [b]Department of Inorganic and Analytical Chemistry,
[c]Department of Engineering Chemistry, Andhra University, Visakhapatnam, 530003, India
avrtoavr@gmail.com

Abstract: Mn substituted LiTi$_2$(PO$_4$)$_3$ samples of composition LiMn$_x$Ti$_{2-x}$(PO$_4$)$_3$ (x=0.0, 0.1, 0.3 and 0.5) have been prepared by solid-state method. XRD studies indicated formation of phase pure materials of rhombohedral structure. Micro structural studies by scanning electron microscopy (SEM) revealed particle size in the range of microns. Conductivity results from 313 K to 573 K showed high ionic conductivity for low amount of Mn and electronic conductivity results are well correlated with ionic conductivity studies. Cyclic voltammetry results showed its electrochemical stability and reaction mechanism in the voltage range from 0.5 to 3.5 V.

Introduction

Exploitation of insertion oxides as host materials for rechargeable batteries has been the subject of many researchers to power several portable electronic devices such as cell phones, laptops, digital cameras *etc.* Since no other cations except H$^+$ can penetrate easily into solids than Li$^+$, the study of rechargeable Li batteries has been actively pursued since 1970s with lithium insertion electrodes in the form of layered LiCoO$_2$ and spinel type LiMn$_2$O$_4$[1-3]. Besides these two host materials, complex phosphates like LiTi$_2$ (PO$_4$)$_3$ (LTP) with NASICON [Na$_3$Zr$_2$ (SiO$_4$)$_2$(PO$_4$)] structure have also been explored because of their high ionic conductivity, low thermal expansion coefficient, and low thermal conductivity[4]. In view of competitive energy-density storage and better thermal properties, phosphate based materials are potential candidates as cathodes for lithium ion batteries compared to traditional cathodes like LiCoO$_2$, LiMn$_2$O$_4$, V$_2$O$_5$, *etc*. LTP structure is made up of two TiO$_6$ octahedra linked with three PO$_4$ tetrahedra via oxygen sharing. Lithium is present in two different types of interstitials formed by six oxygen atoms and eight oxygen atoms respectively. These two interstitials arranged alternatively along the conduction channels provide a three dimensional network for Li-ion transport[5]. The conductivity of these materials

is further increased by heterovalent doping[6]. Several approaches have been developed to improve the electrochemical properties of LTP in terms of substitution of ions such as Al, Zr, Fe, La in Ti site or by increase of Li content in the unit cell[7] or by generating oxygen vacancies in the lattice[8]. ZHAI Jing *et al.* studied the effect of Mn doping in $Li_3V_2(PO_4)_3/C$ and concluded that, Mn doping effectively improved the cyclic stability and electrochemical performance of the material as cathode[9]. Doretta Capsoni *et al.* studied the effect of Mn^{2+} on the electrical properties of LTP in the form of $Li_{1-x/2}Mn_xTi_{2-x/2}$ $(PO_4)_3$ with the supposition that Mn distributes evenly between Li and Ti sites[10]. The present paper describes the effect of Mn^{4+} substitution in the form of $Li(Ti_{2-x}Mn_x)(PO_4)_3$ on the electrochemical properties of LTP.

Experimental

$LiMn_xTi_{2-x}(PO_4)_3$ samples with x=0.0,0.1, 0.3 and 0.5 are synthesized by conventional solid-state method. Stoichiometric amounts of Li_2CO_3, TiO_2, $NH_4H_2PO_4$ and MnO_2 for each composition were finely ground in an agate mortar in presence of methanol for 6 h to obtain homogeneous mixture. The powder was then calcined at 900 ^{0}C for 4 h with a heating rate of 5 ^{0}C per minute. Calcined powder which is white in colour was pressed into pellets using PVA as binder and the pellets were sintered at 1323^{0}K for 2 h on Pt foil.

Phase identification of calcined and sintered powders was performed on D8 ADVANCE Diffractometer of BRUKER AXS with Cu Kα 1 radiation (λ=1.5406 A^0), in the 2θ range from 10^0 to 70^0 in steps of 0.02^0. Experimental densities of LTP and Mn doped LTP pellets were measured at room temperature using standard Archimedes principle. Morphology of fractured surfaces of pellets was examined by JEOL-JSM 6610LV Scanning Electron Microscope (SEM). Raman spectra are recorded on a RAMAN HORIBA JOBIN YVON-LABRAM-HR 800 Raman Spectrometer in the frequency range 50-1200 cm^{-1}. Ionic conductivity studies are made on pellets of 12 mm diameter and 1.5 - 2.5 mm thickness and the measurements were carried out on a HIOKI 3532-50 LCR HITESTER LCR meter in the frequency range from 50 Hz to 1 MHz and in the temperature range from 313 K to 573 K. Electronic conductivities are noted using DMM by MT 4090 LCR/ESR meter in the temperature range from 303 K to 523 K. In order to understand the electrochemical window of the solid state electrolyte LTP, a simple method of cyclic voltammetry has been carried out. The active material was coated on steel foil (cell) is placed in Swagelok setup containing 1M $LiPF_6$ dissolved in ethylene carbonate and dimethyl carbonate (1:1, volumetric ratio). Lithium metal was used as both counter and reference electrodes. The entire cell setup was assembled in an argon-filled glove box and tested with Biologic potentiostat/ galvanostat model VMP3 at a scan rate of 0.1 mV / s for three cycles between 0.5 V to 3.5 V.

Results and Discussion

XRD patterns of LTP precursor powder heat treated at 600, 800 and 900 ^{0}C for 4 h and at 1050 ^{0}C for 2 h are shown in Figure 1. From the XRD data, it is evident that the formation of $LiTi_2$ $(PO_4)_3$ starts at 600 ^{0}C but the reaction does not seem to be complete at this temperature as evidenced by some extra peaks indicated therein. The intensities of these peaks decreased with increase in heat treatment temperature from 600 to 900 ^{0}C and are absent with heat treatment at 1050 ^{0}C. XRD pattern of this corresponded to phase pure LTP of rhombohedral structure and all the observed peaks could be indexed as per JCPDS Card No. 35-0754. XRD patterns of $LiMn_xTi_{2-x}(PO_4)_3$ with $x = 0.1$, 0.3 and 0.5 powders heat treated at 1050 ^{0}C for 2 h depicted in Figure 2 are also in agreement with the XRD pattern for LTP ($x = 0.0$) indicating the formation of single phase compounds.
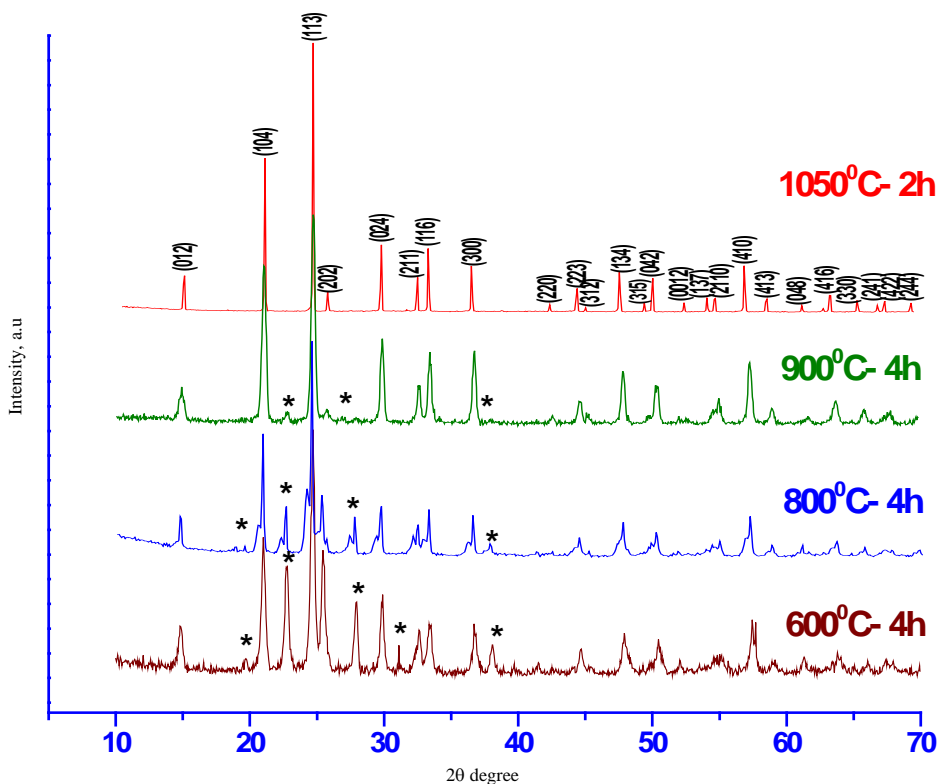
Figure 1. X-ray diffraction patterns of LTP precursor powder heat treated different temperatures
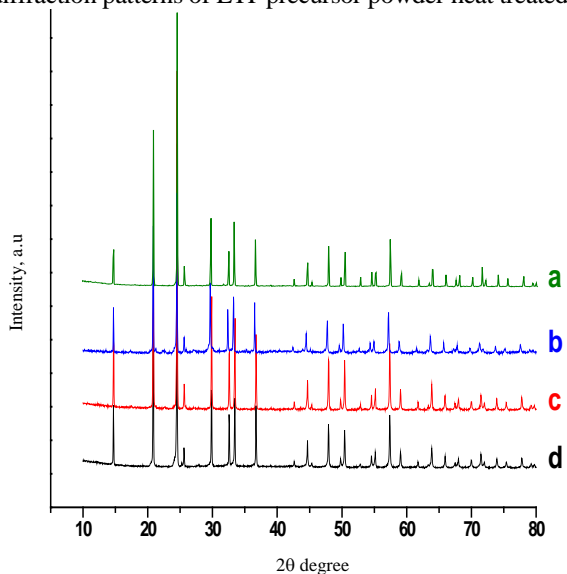
Figure 2. X-ray diffraction patterns of LiMn$_x$Ti$_{2-x}$ (PO$_4$)$_{3,}$ *(a)* x = 0.0, *(b)* x =0.1, *(c)* x = 0.3, *(d)* x = 0.5 precursor powders heat treated at 1050^0 for 2 h

Cell parameters *a* and *c* were calculated using UNITCELL software (Unit-Cell software, 1995) are shown in Table 1. Pure LTP sample powder is white in colour while Mn doped samples are light gray colored and as Mn concentration increased the colour intensity also increased from light gray to thick gray. Lattice parameters of LTP calculated from the XRD data listed in Table 1 agree with earlier reports of crystallographic data[11-13].

Table 1. Calculated lattice parameters and densities for LTP and Mn doped LTP samples

Sample Name	a (A^0)	c (A^0)	c/a (A^0)	Experimental density, g/cm^3	Theoretical density, g/cm^3	Relative density, %
LiTi$_2$ (PO$_4$)$_3$	8.5135	20.8705	2.4514	2.76	2.948	93.6
Li Mn$_{0.10}$Ti$_{1.90}$ (PO$_4$)$_3$	8.5118	20.8771	2.4527	2.74	2.952	92.8
Li Mn$_{0.30}$Ti$_{1.70}$ (PO$_4$)$_3$	8.5107	20.8080	2.4449	2.76	2.975	92.8
Li Mn$_{0.50}$Ti$_{1.50}$ (PO$_4$)$_3$	8.5104	20.8014	2.4442	2.79	2.982	93.6

Raman spectra of LTP and Mn doped LTP samples are shown in Figure 3 from which, it can be seen that four intense peaks appear at 967, 986, 1005 and 1038 cm^{-1} along with two other peaks at 1070 and 1092 cm^{-1}. The peak at 1005 cm^{-1} is due to the symmetric stretching mode of PO_4^{3-} while the peaks at 442 and 432 cm^{-1} are due to the symmetric bending modes. Bands below 350 cm^{-1} are due to external modes and are difficult to be assigned because of mixing.
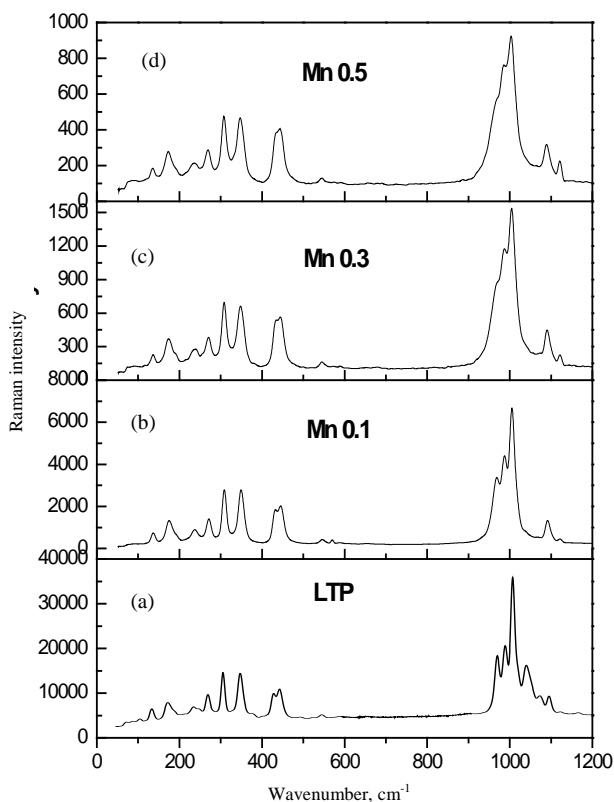
Figure 3. Raman spectra of LiMn$_x$Ti$_{2-x}$ (PO$_4$)$_3$, *(a) x* = 0.0, *(b) x* =0.1, *(c) x* = 0.3, *(d) x* = 0.5 sintered powders

Raman spectra obtained for LTP agree well with report of Burba[14]. Mn sustitution into LTP showed several observable changes on asymmetric stretching modes. Peaks at 967 cm^{-1} and 986 cm^{-1} slowly merged into a single more intense peak with the increase in Mn content. All high intense peaks got slightly shifted to lower wavenumber side with a simultaneous increase in intensity of peaks at 1091,1121 cm^{-1}.

Figure 4 shows SEM images of fractured surfaces of pellets of LTP and Mn doped LTP sintered at 1050 ^{0}C for 2 h. From the SEM micrographs it can be noticed that the grain size considerably increased with increase in Mn content. Cole-Cole plots for 0.1 Mn doped LTP sample given in Figure 5 show a broadened semicircle in the high frequency region at low temperature and the size of semicircle decreased with increasing temperature. With increase in Mn doping up to 0.5, the same trend is observed.

a   b   c
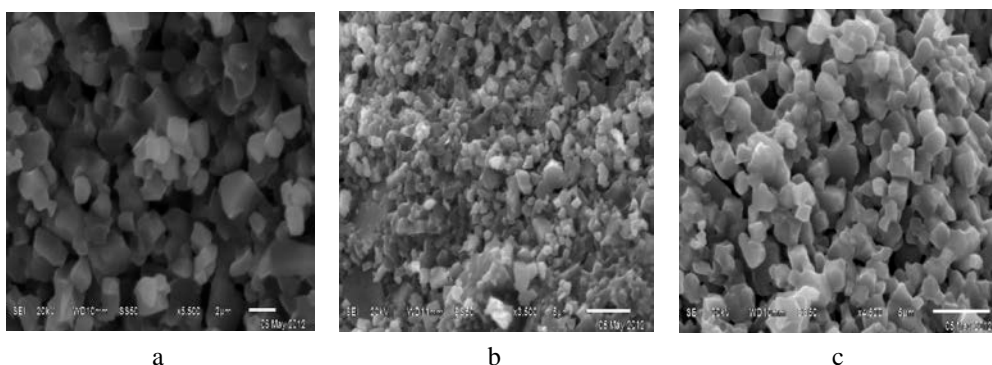
Figure 4. SEM micrographs of fractured surfaces of LiMn$_x$Ti$_{2-x}$ (PO$_4$)$_3$ pellets sintered at 1050^0 for 2 h with *(a) x = 0.0, (b) x =0.1, (c) x = 0.3, (d) x = 0.5*
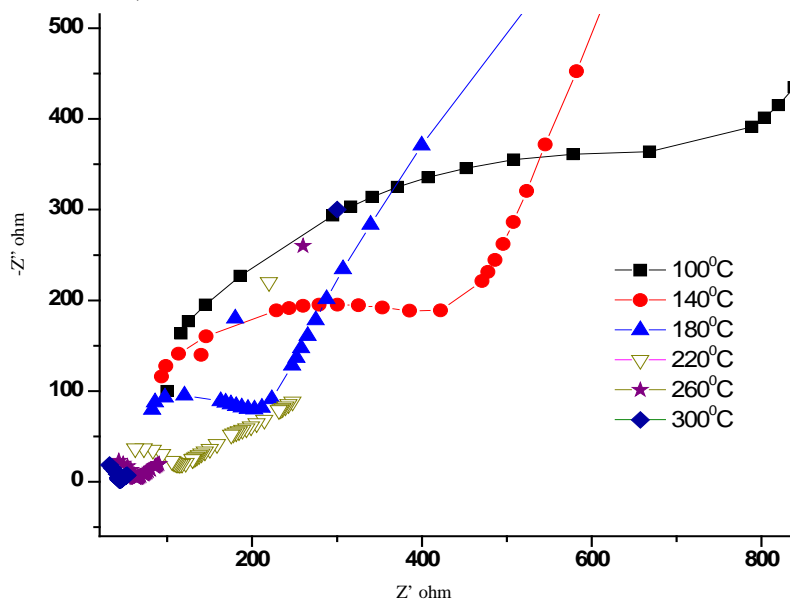
Figure 5. Cole-Cole plots of Li Mn$_{0.1}$Ti$_{1.90}$(PO$_4$)$_3$ at different temperatures (local pattern)

Figure 6 depicts variation of a.c conductivity with temperature for LTP and Mn doped LTP samples. Ionic conductivity of 1.59×10^{-4} S/cm was observed for $LiMn_xTi_{2-x}(PO_4)_3$ with $x = 0.1$ and decreased with increase in concentration of $x > 0.1$. But all the Mn doped samples showed higher conductivity compared to LTP. The a.c conductivity is calculated using the following equation;

$$\sigma_{a.c} = \varepsilon' \varepsilon_o \omega \tan \delta \ (S/cm)$$
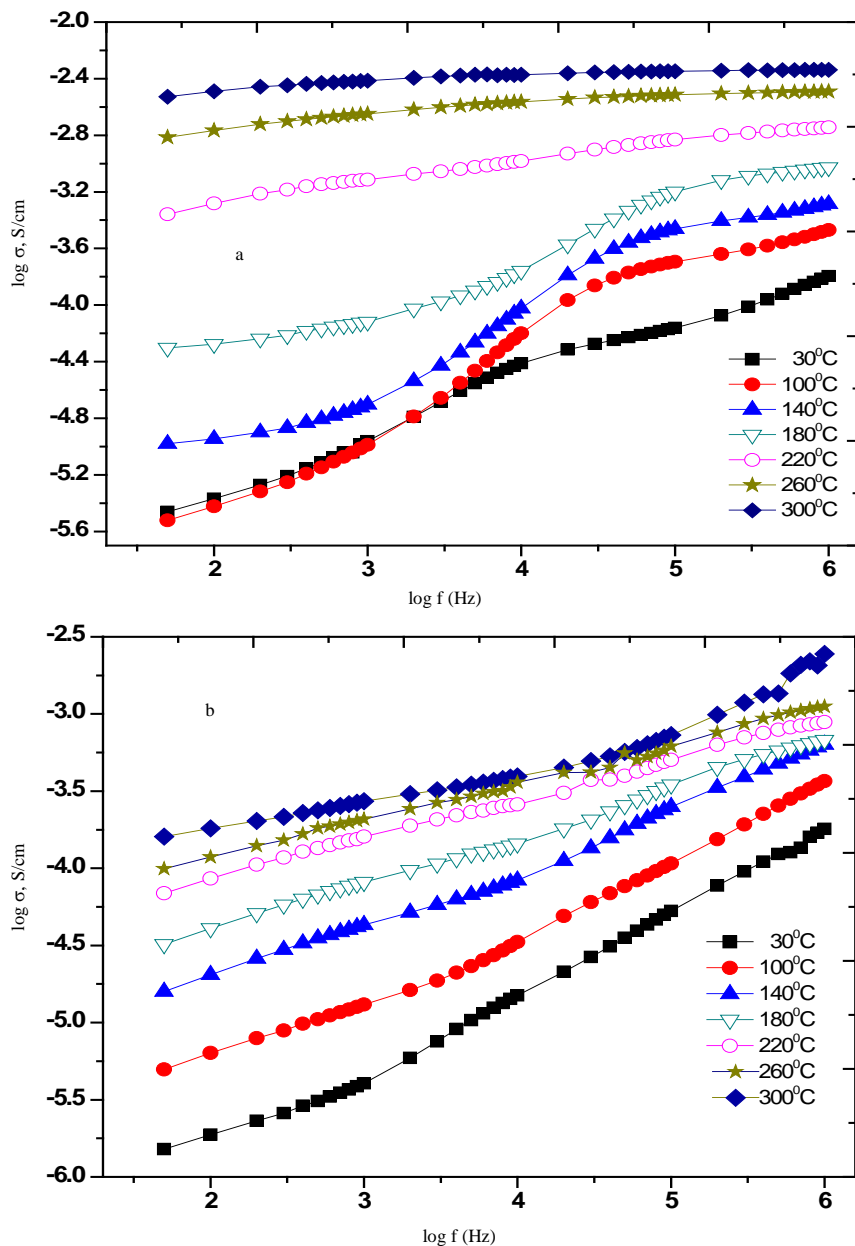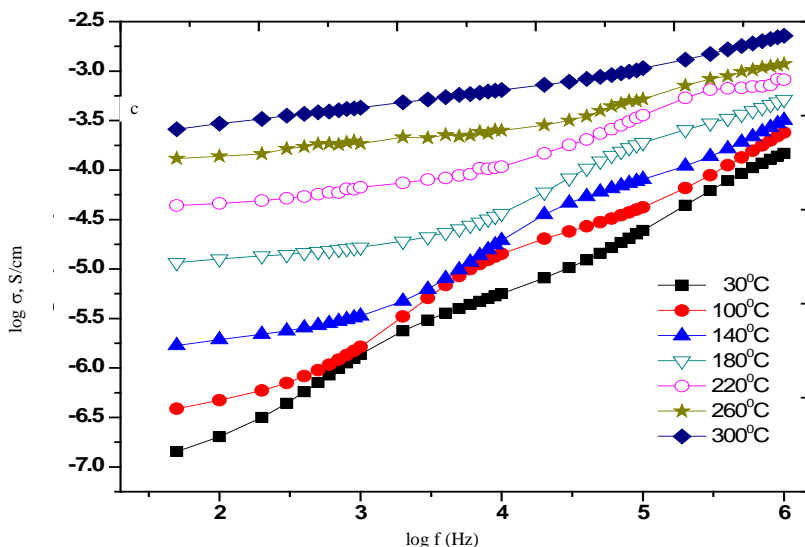
Figure 6. Variation of a.c conductivity of $LiMn_xTi_{2-x}(PO_4)_3$ samples with temperature (Where a = Mn 0.1, b= Mn 0.3 and c = Mn 0.5)

Where ε' is the relative dielectric constant, ε_o is the permittivity in vacuum, ω is $2\pi f$ and tanδ is the dielectric loss. The measured d.c conductivity was found to be 1.23x10⁻⁶ (S/cm). The reason for higher a.c conductivity as compared to d.c conductivity for undoped LTP was explained elsewhere[15]. Figure 7 shows the cyclic voltammogram of Li $Mn_{0.10}Ti_{1.90}(PO_4)_3$ sample. Initially the reduction peak is observed at 2.08 V, but the reduction peaks are stabilized at 2.42 V. The oxidation peaks are observed at 2.55 V. The difference between reduction and oxidation voltages is 0.13 V. This voltage difference is less than that observed for undoped $LiTi_2(PO_4)_3$ (0.24V). The peak intensities and electrochemical reactivity of Mn doped samples is higher than that of LTP. The data obtained suggest that electrochemical properties are improved with Mn 0.1 doping in LTP.
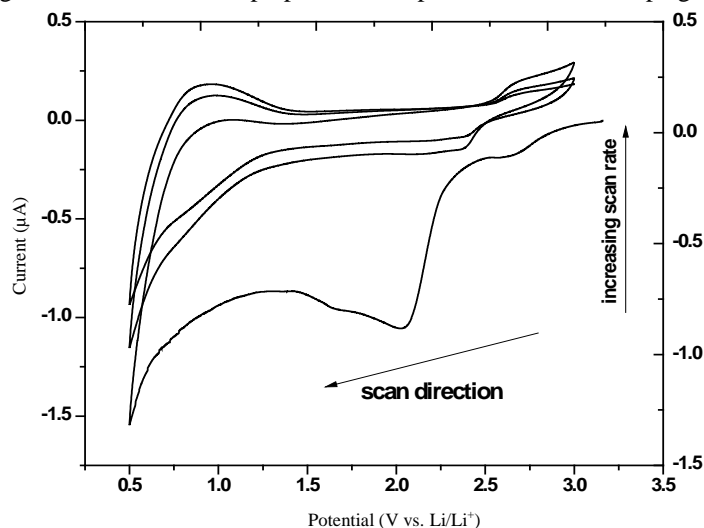
Figure 7. Cyclic voltammogram of Li $Mn_{0.10}Ti_{1.90}(PO_4)_3$

Conclusion

Powders of different compositions corresponding to Li Mn_xTi_{2-x} $(PO_4)_3$ (x=0.0, 0.1, 0.3 and 0.5) have been prepared by conventional solid-state method. XRD patterns of LTP heat treated at 600, 800, 900 ^{0}C for 4 h and 1050 ^{0}C for 2 h showed formation of phase pure LTP with rhombohedral symmetry at 1050 ^{0}C. Mn-substitution in LTP led to observable shift of high intense bands to low wave number side along with an increase in intensity of peaks at 1091, 1121 cm^{-1} in the Raman spectra. SEM micrographs showed grain size of samples increased with increase in Mn content. The ionic conductivity at room temperature is 1.59×10^{-4} S/cm. A.C condctivity studies indicated that low concentration of Mn is more effective compared to Mn concentration $0.1< x <0.5$. The measured d.c conductivity was 1.23×10^{-6} S/cm. From cyclic voltammetry results it could be seen that Mn concentration of $x = 0.1$ is good for enhancing the electrochemical properties of LTP.

References

1.   Hong H Y P, *Mater Res Bull.*, 1976, **11**, 173-182.
2.   Kasturi Rangan K and Gopalakrishnan J, *J Solid State Chem.*, 1994, **109(1)**, 116-121.
3.   Aono H, Sugimoto E, Sadaoka Y, Imanaka N and Adachi G-Y, *J Electrochem Soc.,* 1990, **137**, 1023.
4.   Goodenough J B, Hong H Y P and Kafalas J A, *Mater Res Bull.*, 1976, **11**, 203-220.
5.   Wolfenstine J, Foster D, Read J and Allen J L, *J Power Sources.*, 2008, **182**, 626.
6.   Pinus I Yu, Stenina I A, Rebrov A I, Zhuravlev N A and Yaroslavtsev A B, *Russian J Inorg Chem.*, 2009, **54(8)**, 1177-1180.
7.   Kazakevicius E, Salkus T, Dindune A, Kanepe Z, Ronis J, Kezionis A, Kazlauskiene V, Miskinis J, Selskiene A and Selskis A, *Solid State Ionics*, 2008, **179(1-6)**, 51-56.
8.   Li-Juan Chen, Yu-Jun Zhao, Jia-Yan, Jia-Yan Luo and Yong-Yao Xia, *Physics Letters A,* 2011, **375(5)**, 934-938.
9.   ZHAI jing, ZHAO Min-shou and WANG Dan-dan, *Trans Nonferrous Met Soc China*, 2011, **21(3)**, 523-528.
10.   Doretta Capsoni, Marcella Bini, Stefania Ferrari, Piercarlo Mustarelli, Vincenzo Massarotti, Maria Cristina Mozzati and Alberto Spinella, *J Phys Chem C*, 2010, **114(32)**, 13872-13878.
11.   Aatiq, Menetrier M, Croguennec L, Suard E and Delmas C, *J Mater Chem.*, 2002, **12**, 2971-2978.
12.   Wang G X, Bradhurst D H, Dou S X and Liu H K, *J Power Sources*, 2003, **124**, 231-236.
13.   Joint Commission on Powder Diffraction Standards (JCPDS) Card No. 35-754, International Centre for Diffraction Data, Newtown Square, PA, USA.
14.   Burba C M and Frech R, *Solid State Ionics*, 2006, **177**, 1489.
15.   Ramaraghavulu R and Buddhudu S, *Ceramics International*, 2011, **37**, 3651.